Hindawi
International Transactions on Electrical Energy Systems
Volume 2023, Article ID 8352768, 13 pages
https://doi.org/10.1155/2023/8352768

Research Article

A Bi-Level Optimization Model for Flexible Capacity Allocation with Coordinated Planning and Operation

Xinyu Yin[1], **Xiaoyan Bian**[1], **Qinran Zhu**[2], **Jinbin Zhao**[1], **Shunfu Lin**[1] and **Kwok L. Lo**[3]

[1]*Electrical Engineering College, Shanghai University of Electric Power, Shanghai, China*
[2]*State Grid Ningbo Power Supply Company, Zhejiang, China*
[3]*Faculty of Engineering, University of Strathclyde, Glasgow, UK*

Correspondence should be addressed to Xiaoyan Bian; bianxy@shiep.edu.cn

Received 12 July 2023; Revised 24 November 2023; Accepted 18 December 2023; Published 31 December 2023

Academic Editor: Michele De Santis

Copyright © 2023 Xinyu Yin et al. This is an open access article distributed under the Creative Commons Attribution License, which permits unrestricted use, distribution, and reproduction in any medium, provided the original work is properly cited.

Traditional methods for flexible capacity allocation do not take into account the actual operation status of resources, and this can lead to redundancy of allocation results in a high renewable penetration power system. Using collaborative optimization during the flexibility resource planning stage can significantly improve the overall economics and flexibility. Therefore, a bilevel operation-planning joint optimization model for flexible capacity allocation is proposed in this paper. The aim is to optimize the annual total cost and flexibility of the system. The upper planning level introduces the economic costs, flexibility resource capacity, and flexibility index which are used as the evaluation index of system flexibility, while in the lower operation level, a morphological clustering algorithm based on the multiscale and entropy weight method is proposed for obtaining typical scenarios of flexibility demand. On this basis, the lower level simulates production to estimate daily operating costs. In addition, the model is solved iteratively using the nondominated sorting genetic algorithm-II (NSGA-II) and the linear programming method to obtain the Pareto solutions. Case studies are carried out based on a practical town area, and the results verify the validity and rationality of the proposed bilevel capacity allocation model.

1. Introduction

Due to the random volatility of high penetration with intermittent or weather-dependent renewable energy, traditional energy sources [1] can no longer meet the flexibility needs and keep the supply-demand balance of the power system. Therefore, it is necessary to carry out research on the flexibility and optimized allocation of flexible resources.

Several academics have already undertaken research on the concept and assessment of flexibility of the high renewable penetration power system. The International Energy Agency (IEA) defines flexibility as "the ability of a power system to reliably and cost-effectively manage the variability and uncertainty of demand and supply across all relevant timescales" [2]. The authors in reference [3] proposed a framework based on machine learning to assess the flexibility of power systems. The authors in reference [4] evaluated the flexibility of the system by means of flexibility supply/demand probability convolution. In reference [5], a flexibility metric is introduced into a unit commitment model to quantitatively assess network flexibility. The abovementioned studies have provided useful explorations of flexibility assessment in power systems; however, there is a lack of the application of flexibility assessment in flexible capacity allocation, where flexible capacity refers to the capacity of multiple flexibility resources in the system.

Recently, research has been conducted on the allocation of flexible resources for the high renewable penetration power system. Transformation measures of the thermal power plant on improving the flexible regulation capability of the system were explored in references [6, 7]; the abovementioned studies only consider the impact of flexibility of a single resource. The authors in reference [8] implemented a single-level model for generation and transmission expansion planning, primarily focused on

minimizing the cost of the system. However, this approach is characterized by its simplicity and limited versatility. In reference [9], a single-level allocation model was developed for flexible resources on the source-load side, taking into account the demand in peaking scenarios. However, this model does not include the operational state of resources and allocates them based on a single scenario, potentially resulting in cost-ineffective allocation results. Therefore, the bilevel optimization model considering both planning and operation is a necessity.

Few papers carried out research on the bilevel allocation model for flexible resources. The authors in reference [10] proposed an optimal allocation model of community-integrated energy systems, but it did not quantify the demand and supply of the flexibility. In [11, 12], a multitimescale energy storage system (ESS) planning model based on bilevel decision-making is proposed, and it did not take into account the advantages of joint optimization of various flexibility resource types and only accomplished allocation within a single scenario, thereby restricting the versatility of the model. Furthermore, few research has been uncovered that achieves multiobjective optimization of economics and flexibility. In recent years, there have been significant advances in the study of algorithms used to solve multiobjective optimization problems; the authors in reference [13] provided the decomposition-based multiobjective optimization evolutionary algorithms (MOEA/D). The NSGA-II in reference [14] presented three major improvements to the NSGA algorithm, including nondominated sorting, crowding distance, and elite preserving strategy, to enhance the computational efficiency of the algorithm.

The previous sections discussed a literature review of the resource allocation method, including allocation scenarios, models, and solution algorithms. It is found important to consider both planning and operations to achieve flexible capacity allocation in typical scenarios. Accordingly, the main contributions of this paper are summarized as follows:

(1) An operation-planning joint optimization model for flexible resources that considers both investment decisions and optimal operation is established, significantly increasing the overall economics and flexibility of the system and avoiding redundancy in resource allocation.

(2) A morphological clustering algorithm based on the multiscale and entropy weight method is proposed for obtaining typical days which consider the morphological characteristic of the curves. This algorithm aims to identify typical days that can serve as typical scenarios for flexibility resource allocation.

(3) The Pareto principle is utilized to combine the economics and flexibility into the objective function and effectively solve the problem without setting the weight coefficients of economics and flexibility.

The remainder of this paper is organized as follows. In Section 2, a morphological clustering algorithm based on the multiscale and entropy weight method is proposed for the selection of typical scenarios of flexibility demand. A bi-level operation-planning joint optimization model for flexible resources is established in Section 3 and realizes the flexible capacity allocation by recursive iteration between the upper and lower levels. Section 4 validates the abovementioned model with the actual data. Section 5 summarizes the conclusions.

2. Typical Scenarios of the Flexibility Demand Based on the Morphological Clustering Algorithm

The curves of the net load of the high renewable penetration power system are multitemporal and fluctuating. The morphological similarity between curves can be depicted through the difference-measure matrix and the entropy weight approach. Therefore, the morphological clustering algorithm is used to cluster the net load curves.

The principle and function of the morphological clustering algorithm are to cluster the net load curves into several typical scenarios for flexibility resource allocation according to the characteristic of morphologic. The algorithm in this paper consists of four modules based on morphological distances, namely, data preprocessing, feature matrix calculation, difference metric matrix calculation, and the K-means approach [15, 16] to identify the center of clustering.

2.1. Data Preprocessing. Curve smoothing and the deletion of spurious data are both included in the data preprocessing. Taking the net load data of a province for n days as a sample, the values with large deviations are modified.

Due to the volatility of renewable energy, the polynomial interpolation method is used to smooth the curve of the original data. This method can more adequately describe the overall trend of the curve and overcome the influence of fluctuations on clustering.

After data preprocessing, the initial data matrix can be obtained for further data processing as follows:

$$\mathbf{X} = \begin{bmatrix} x_{1,1} & x_{1,2} & \cdots & x_{1,m} \\ x_{2,1} & x_{2,2} & \cdots & x_{2,m} \\ \vdots & \vdots & \ddots & \vdots \\ x_{n,1} & x_{n,2} & \cdots & x_{n,m} \end{bmatrix}, \tag{1}$$

where x_{ij} is the output data at time j on day i, with $i = 1 \sim n$, $j = 1 \sim m$.

2.2. Other Recommended Morphological Characteristic Matrices. In this paper, the four different distances are used to better describe the morphological characteristics of the curve. The feature matrix is obtained to describe the morphological characteristics of the n-day daily output curve.

According to the original data matrix $\mathbf{X}$, the curve of the net load is divided into m-1 segments and calculated the difference value of each segment separately to get the adjacent difference matrix $\mathbf{X_1}$ as follows:

$$\mathbf{X}_1 = \begin{bmatrix} x_{1_{1,1}} & x_{1_{1,2}} & \cdots & x_{1_{1,(m-1)}} \\ x_{1_{2,1}} & x_{1_{2,2}} & \cdots & x_{1_{2,(m-1)}} \\ \vdots & \vdots & \ddots & \vdots \\ x_{1_{n,1}} & x_{1_{n,2}} & \cdots & x_{1_{n,(m-1)}} \end{bmatrix}, \tag{2}$$

where $x_{1i,j} = x_{i,(j+1)} - x_{i,j}$.

Then, we calculated the six-segment difference matrix $\mathbf{X_2}$.

$$\mathbf{X}_2 = \begin{bmatrix} x_{2_{1,1}} & x_{2_{1,2}} & \cdots & x_{2_{1,6}} \\ x_{2_{2,1}} & x_{2_{2,2}} & \cdots & x_{2_{2,6}} \\ \vdots & \vdots & \ddots & \vdots \\ x_{2_{n,1}} & x_{2_{n,2}} & \cdots & x_{2_{n,6}} \end{bmatrix}, \tag{3}$$

where $x_{2i,j} = x_{i,((\mathrm{mj}/6)+1)} - x_{i,((\mathrm{m}(j-1)/6)+1)}$.

Similarly, the three-segment difference matrix $\mathbf{X_3}$ and the head-to-tail difference distance matrix $\mathbf{X_4}$ can be calculated.

For the difference matrix $\mathbf{X_k}$ ($k = 1, 2, 3, 4$), we set the number of quantile points to 3 [17] and the confidence probability values are 0.1, 0.5, and 0.9, respectively. Let the characteristic matrix extracted from the morphological characteristics of the curve be $\mathbf{Y_k}$, where the elements are as follows:

$$y_{k_{i,j}} = \begin{cases} 3, x_{k_{i,j}} > 0.9\max(\mathbf{X}_k), \\ 2, 0.5\max(\mathbf{X}_k) < x_{k_{i,j}} < 0.9\max(\mathbf{X}_k), \\ 1, 0.1\max(\mathbf{X}_k) < x_{k_{i,j}} < 0.5\max(\mathbf{X}_k), \\ 0, 0.1\min(\mathbf{X}_k) < x_{k_{i,j}} < 0.1\max(\mathbf{X}_k), \\ -1, 0.5\min(\mathbf{X}_k) < x_{k_{i,j}} < 0.1\min(\mathbf{X}_k), \\ -2, 0.9\min(\mathbf{X}_k) < x_{k_{i,j}} < 0.5\min(\mathbf{X}_k), \\ -3, x_{k_{i,j}} < 0.9\min(\mathbf{X}_k). \end{cases} \tag{4}$$

$\mathbf{Y_1}$ reflects the intensity of change of adjacent sampling points. $\mathbf{Y_2}$ reflects the fluctuation characteristics of six segments throughout the day. $\mathbf{Y_3}$ is the matrix that characterizes the segmentation trend. $\mathbf{Y_4}$ reflects the difference in output at the beginning and at the end of the day.

2.3. Difference-Measure Matrix. In this paper, the morphological differences of the curves at different scales are described by the metric matrices $\mathbf{D_1}$, $\mathbf{D_2}$, $\mathbf{D_3}$, and $\mathbf{D_4}$ corresponding to $\mathbf{Y_1}$, $\mathbf{Y_2}$, $\mathbf{Y_3}$, and $\mathbf{Y_4}$, respectively, and the elements of which are shown as follows:

$$\begin{aligned} d_{1_{i,j}} &= \sum_{l=1}^{n} \left(y_{1_{i,l}} - y_{1_{j,l}} \right), \\ d_{2_{i,j}} &= \sum_{l=1}^{6} \left(y_{2_{i,l}} - y_{2_{j,l}} \right), \\ d_{3_{i,j}} &= \sum_{l=1}^{4} \left(y_{3_{i,l}} - y_{3_{j,l}} \right), \\ d_{4_{i,j}} &= y_{4_{i,l}} - y_{4_{j,1}}. \end{aligned} \tag{5}$$

Taking $\mathbf{D_1}$ as an example, $y_{1i,l} - y_{1\,j,l}$ represent the difference of eigenvalues in the period l of day i and day j and then sums the difference values of n periods throughout the day.

Then, we defined the difference-measure matrix $\mathbf{D}$ as follows:

$$\mathbf{D} = \omega_1 \mathbf{D}_1 + \omega_2 \mathbf{D}_2 + \omega_3 \mathbf{D}_3 + \omega_4 \mathbf{D}_4, \tag{6}$$

where ω_1, ω_2, ω_3, and ω_4 are the weights to be determined in the next section.

2.4. Weight Assignment Based on the Entropy Weight Method. The entropy weight approach is commonly used to objectively assign weights to indicators based on the data [18, 19].

First, determine the entropy. The value of entropy represents the difference between various indicators. The higher the entropy value, the smaller the corresponding degree of difference and the weight [20]. The entropy of the indicator k is determined by the following two formulas:

$$\begin{aligned} h_m &= -\frac{1}{\ln n} \sum_{n=1}^{n} f_{\mathrm{mn}} \ln f_{\mathrm{mn}}, \\ f_{\mathrm{mn}} &= \frac{r_{\mathrm{mn}}}{\sum_{n=1}^{n} r_{\mathrm{mn}}}, \end{aligned} \tag{7}$$

where $n = 1, 2, 3, 4$. r_{mn} is the actual data of the evaluation object n under the indicator m; $f_{\mathrm{mn}} f_{\mathrm{mn}}$ is the contribution degree of the evaluation object n under the indicator m.

Second, ω_u is expressed as follows, with $u = 1, 2, 3, 4$:

$$\omega_u = \frac{e^{\left(\sum_{t=1}^{n} h_t + 1 - h_m\right)} - e^{(h_m)}}{\sum_{l=1}^{n} \left(e^{\left(\sum_{t=1}^{n} h_t + 1 - h_m\right)} - e^{(h_m)} \right)}. \tag{8}$$

3. Bi-level Operation-Planning Joint Optimization Model

A bi-level operation-planning joint optimization model is proposed in this paper to optimize the capacity allocation of various flexible resources. In this section, a detailed description is provided for the framework of the model, including the upper-level investment decision model, the lower-level optimization operation model, and the solution algorithm.

3.1. The Framework of the Bi-level Operation-Planning Joint Optimization Model. The bi-level optimization of flexible resources considers both the planning and the operation. The traditional allocation method is prone to problems, such as high dimensionality and redundancy of capacity. As a result, the flexible resources may not be optimally utilized and the overall economics of the system may be compromised.

The flexibility resource optimization model established in this paper decomposes the objective problem into the following two subproblems: flexibility resource investment decision and operation simulation.

Based on the typical scenarios of the flexibility demand, the upper level determines the annual total cost and the flexibility index as the objective. The obtained allocation schemes can then be used as inputs for the lower-level subproblem that considers the operational simulation and optimizes the operational costs and the flexibility index of the typical day. It provides the results of operation for the upper level. The model is able to find a set of Pareto optimal solution sets through a limited number of iterations.

The framework of the bilevel model is shown in Figure 1. A bi-level model facilitates the use of different solution algorithms for the upper and lower levels. In this way, it improves computational efficiency and obtains the flexibility resource allocation scheme that meets the overall objective of economy and flexibility.

3.2. Investment Decision Problems in the Upper Level. The upper level is a multiobjective optimization problem that meets the optimal annual total cost and flexibility of the system. The capacity of each type of flexibility resource is determined as the decision variable, and its solution of capacity allocation is used as the input condition of the lower-level sub-problem.

3.2.1. Objective Function. The objective function of the upper level consists of the annual investment cost, annual operation cost, and compensation cost of the interruptable load. The weights of each type of flexibility resource as well as the probability of each typical daily scenario are also considered.

$$\min C = C_{\text{inv}} + C_{\text{oper}} + C_{\text{dsm}}, \tag{9}$$

$$\min f = \text{flex}, \tag{10}$$

$$C_{\text{inv}} = \frac{i(1+i)^m}{(1+i)^m - 1} \times \left(\alpha_1 C_g + \alpha_2 C_T + \alpha_3 C_{\text{hy}} + \alpha_4 C_{\text{ESS}} + \alpha_5 C_{\text{pump\_sto}} + \alpha_6 C_{\text{int\_load}}\right), \tag{11}$$

$$C_{\text{oper}} = \sum_{s=1}^{N_s} n_s C_{\text{oper},s}, \tag{12}$$

$$C_{\text{dsm}} = \sum_{s=1}^{N_s} n_s C_{\text{dsm},s}, \tag{13}$$

$$\text{flex} = \sum_{s=1}^{N_s} n_s f_{\text{flex}}, \tag{14}$$

where C is the total cost, C_{inv} is the investment cost, C_{oper} is the annual operating cost of the system, and C_{dsm} is the compensation cost of the interruptable load. C_g, C_T, C_{hy}, C_{ESS}, $C_{\text{pump}_{\text{hy}}}$, and $C_{\text{int\_load}}$ are the investment costs of thermal power, thermal unit flexibility modification, hydropower, energy storage, pumped storage, and interruptable load, respectively. α_1, α_2, α_3, α_4, α_5, and α_6 are the weight coefficients of each resource category based on the principal component analysis [21], summing to 1. i is the discount rate, taken as 0.08, and m is the investment planning period of each resource. $C_{\text{oper},s}$ and $C_{\text{dsm},s}$ are the daily operating cost and the compensation cost of typical scenario s. n_s is the number of typical days in a year with scenario number s. f_{flex} is a flexibility index defined in equation (14), which serves as a quantitative measure to evaluate the level of flexibility during system operation.

The cost of each type of flexible resource is calculated as follows:

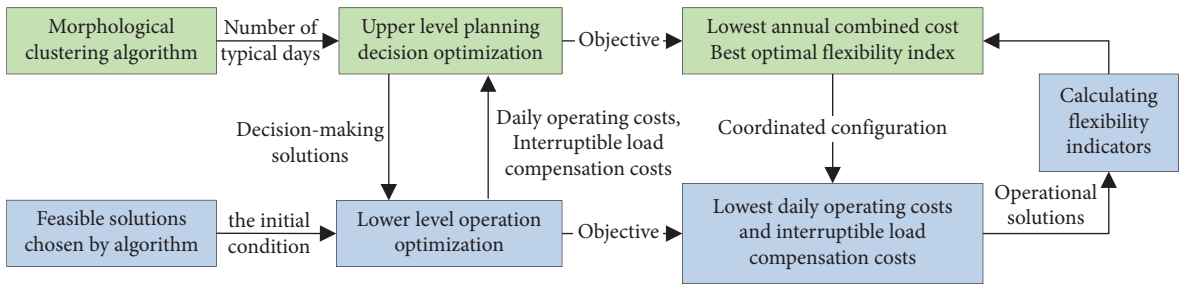

Figure 1: Framework of the bi-level operation-planning joint optimization model.

$$\begin{aligned} C_{\mathrm{g}} &= \lambda_{\mathrm{coal}} Cap_{\mathrm{coal}} + \lambda_{\mathrm{gas}} Cap_{\mathrm{gas}}, \\ C_T &= \lambda_T Cap_T, \\ C_{\mathrm{hy}} &= \lambda_{\mathrm{hy}} Cap_{\mathrm{hy}}, \\ C_{\mathrm{ESS}} &= \lambda_{\mathrm{ESS}} Cap_{\mathrm{ESS}}, \\ C_{\mathrm{pump\_hy}} &= \lambda_{\mathrm{pump\_hy}} Cap_{\mathrm{pump\_hy}}, \\ C_{\mathrm{int\_load}} &= \lambda_{\mathrm{int\_load}} Cap_{\mathrm{int\_load}}, \end{aligned} \tag{15}$$

where λ_{coal}, λ_{gas}, λ_T, λ_{hy}, λ_{ESS}, $\lambda_{\mathrm{pump\_hy}}$, and $\lambda_{\mathrm{int\_load}}$ are the unit investment costs for coal, gas, thermal unit flexibility retrofit, hydro, storage, pumped storage, and interruptable load, respectively. Cap_{coal}, Cap_{gas}, Cap_T, Cap_{s}, Cap_{ESS}, $Cap_{\mathrm{pump\_hy}}$, and $Cap_{\mathrm{int\_load}}$ are the planned capacities of coal, gas, thermal unit flexibility retrofit, hydro, storage, pumped storage, and interruptable load, respectively.

3.2.2. Constraints. In addition to the maximum and minimum limits of the capacity constraints for flexible resources, there are interruptable load constraints and power demand constraints; they are as follows:

$$Cap_{\mathrm{int\_load}} \le \beta P_{\mathrm{load}}, \tag{16}$$

where β is taken as 5%.

$$\begin{aligned} \left(E_{\mathrm{it}} + E_{\mathrm{kt}}\right)\left(1 - \varepsilon_{\mathrm{loss}}\right) &\ge P_{\mathrm{load}_{\max}}, \\ E_{\mathrm{kt}} &= Cap_{\mathrm{coal}} + Cap_{\mathrm{gas}} + Cap_T \\ &\quad + Cap_{\mathrm{hy}} + Cap_{\mathrm{pump\_hy}}, \end{aligned} \tag{17}$$

where E_{it} and E_{kt} indicate the new flexible resources and existing power supply capacity, respectively. $\varepsilon_{\mathrm{loss}}$ is the power supply loss rate, which is generally taken as 10%. In this paper, E_{it} is Cap_T, which is the flexibility transformation capacity of thermal power units.

3.3. Optimization of Operational Problems in the Lower Level. The lower-level optimization operation model optimizes in a day-ahead scheduling for a given flexible resource capacity in the upper level. The optimization variables are the daily output of each type of flexible resource, which is a continuous variable.

3.3.1. Objective Function. The objective function of the lower-level model includes the operating cost of a typical day and the compensation cost of the interruptable load. The details are as follows:

$$\begin{aligned} \min f &= C_{\mathrm{oper},s} + C_{\mathrm{dsm},s}, \\ C_{\mathrm{oper},s} &= \sum_{t=1}^{T} \left(C_g P_{g,t} + C_{\mathrm{ESS}} \left|P_{\mathrm{ESS}}\right|\right) \times \Delta t, \\ C_{\mathrm{dsm},s} &= \sum_{t=1}^{T} c_{\mathrm{int\_load}}^{\mathrm{cut}} P_{\mathrm{int\_load,t}} \Delta t, \end{aligned} \tag{18}$$

where T is the number of periods divided in a day. Δt is the duration of each time slot. In this paper, $\Delta t = 1$ h; daily operation cost, $C_{\mathrm{oper},s}$, includes the generation cost of thermal power, operation, and maintenance cost of energy storage. There is no fuel consumption cost for hydroelectric power units and pumped-storage operation. C_{ESS} is the operation and maintenance cost of energy storage per unit of electricity, and $\mathrm{P}_{\mathrm{ESS}}$ indicates the actual power output of energy storage at time t. $C_{\mathrm{dsm},s}$ is the cost of the interruptable load, $c_{\mathrm{int\_load}}^{\mathrm{cut}}$ is the unit compensation cost, and $P_{\mathrm{int\_load},t}$ is the amount of the interruptable load at a certain time t.

3.3.2. Constraints. The constraints in the lower level are mainly operation constraints and investment-decision constraints including power balance constraints of the system, charging and discharging of ESS, conventional unit, and output of wind and PV.

The power balance constraint is expressed in the following equation:

$$\begin{aligned} P_{g,t} + P_{\mathrm{ESS},t}^{\mathrm{dis}} - P_{\mathrm{ESS},t}^{\mathrm{cha}} + P_{\mathrm{pump\_hy},t} + P_{\mathrm{hy},t} + P_{\mathrm{wind},t} + P_{\mathrm{PV},t} \\ + P_{\mathrm{he},t} + P_{\mathrm{int\_load},t} = P_{\mathrm{load},t}. \end{aligned} \tag{19}$$

The charging and discharging constraints of ESS are expressed in equations (20) and (21). The charging and discharging power limit of ESS cannot exceed the installed capacity. Meanwhile, the charging and discharging process should meet the energy balance of ESS.

$$0 \le P_{\mathrm{ESS},t}^{\mathrm{dis}}, P_{\mathrm{ESS},t}^{\mathrm{cha}} \le Cap_{\mathrm{ESS}}, \tag{20}$$

$$E_{\mathrm{ESS},t} - E_{\mathrm{ESS},t-1} = \eta_{\mathrm{ESS}} P_{\mathrm{ESS},t}^{\mathrm{cha}} - \frac{P_{\mathrm{ESS},t}^{\mathrm{dis}}}{\eta_{\mathrm{ESS}}}. \tag{21}$$

The ramp-up and start-stop constraints for conventional thermal units and hydropower are represented in the following equations restricting that the thermal output does not exceed the installed capacity and it also meets the ramp-up rate limit.

$$0 \le P_t \le Cap, \tag{22}$$

$$-\alpha^{\mathrm{down}} Cap \le P_t - P_{t-1} \le \alpha^{\mathrm{up}} Cap. \tag{23}$$

Pumped-storage units are required to meet the water balance of pumped-storage power plants as well as power generation and pumping power constraints.

$$\sum_{i=1}^{T_G} \left(P_i^{\mathrm{PH}} > 0\right) = -\eta \sum_{i=1}^{N-T_G} \left(P_i^{\mathrm{PH}} < 0\right). \tag{24}$$

The percentage constraint of the interruptable load can be expressed by the following equation, where β is taken as 5% according to the actual situation of the plan.

$$P_{\mathrm{int\_load}} \le \beta P_{\mathrm{load}}. \tag{25}$$

The system power supply adequacy constraint can be expressed by the following equation, where $P_{\mathrm{ld},t}$ is the load of the system at time t and γ is the power supply adequacy.

$$\sum_{t=1}^{N_t} P_{\mathrm{ld},t}^{\mathrm{cut}} \le \gamma \sum_{t=1}^{N_t} P_{\mathrm{ld},t}. \tag{26}$$

3.4. Calculation of the Flexibility Index. The flexibility index is used to determine whether the flexible resources meet the flexibility demand. In the system, wind power and PV are uncontrollable units, while thermal power and the interruptable load are controllable units. In the calculation of flexibility demand, uncontrollable units and loads are considered; in the calculation of flexibility supply, the flexibility supply capacity provided by controllable units and interruptable loads is considered. In this section, the flexibility index is calculated for a typical daily operation scenario.

The flexibility demand is calculated by the following equation:

$$\begin{aligned} P_{\mathrm{uncon\_demand}}(t) &= P_{\mathrm{load}}(t), \\ P_{\mathrm{uncon\_supply}}(t) &= P_{\mathrm{wind}}(t) + P_{\mathrm{PV}}(t), \\ P_{\mathrm{demand}}(t) &= P_{\mathrm{uncon\_demand}}(t) - P_{\mathrm{uncon\_supply}}(t), \end{aligned} \tag{27}$$

and when $P_{\mathrm{demand}}(t) > P_{\mathrm{demand}}(t-1)$, there is a need for upward flexibility.

$$P_{\mathrm{demand\_up}}(t) = P_{\mathrm{demand}}(t) - P_{\mathrm{demand}}(t-1), \tag{28}$$

and when $P_{\mathrm{demand}}(t) < P_{\mathrm{demand}}(t-1)$, there is a demand for downward flexibility.

$$P_{\mathrm{demand\_down}}(t) = P_{\mathrm{demand}}(t-1) - P_{\mathrm{demand}}(t). \tag{29}$$

Flexibility supply is calculated based on the following equations:

$$\begin{aligned} P_{\mathrm{supply\_up}}(t) = {} & \min\left(\alpha_g^{\mathrm{up}} \Delta t, P_{g\_\max} - P_g(t)\right) + \min\left(\alpha_{\mathrm{hy}}^{\mathrm{up}} \Delta t, P_{\mathrm{hy\_max}} - P_{hy}(t)\right) \\ & + \min\left[P_{\mathrm{dis\_max}}, \frac{Cap_{\mathrm{ESS}} \eta_{\mathrm{ESS}} \left(\mathrm{SOC}(t) - SOC_{\min}\right)}{\Delta t}\right] \\ & + \min\left[P_{\mathrm{pump\_hy},+,\max}, \frac{P_{\mathrm{pump\_hy}}(t) - P_{\min}}{\delta}\right] + \min\left(\beta P_{\mathrm{load}}(t) \Delta t, P_{\mathrm{int\_load\_max}}\right), \\ P_{\mathrm{supply\_down}}(t) = {} & \min\left(\alpha_g^{\mathrm{down}} \Delta t, P_g(t) - P_{g\_\min}\right) + \min\left(\alpha_{\mathrm{hy}}^{\mathrm{down}} \Delta t, P_{\mathrm{hy}}(t) - P_{\mathrm{hy\_min}}\right) \\ & + \min\left[P_{\mathrm{cha\_max}}, \frac{Cap_{\mathrm{ESS}} \left(\mathrm{SOC}_{\max} - \mathrm{SOC}(t)\right)}{\eta_{\mathrm{ESS}} \Delta t}\right] \\ & + \min\left[P_{\mathrm{pump\_hy},-,\max}, \frac{P_{\max} - P_{\mathrm{pump\_hy}}(t)}{\delta}\right] + \min\left(\beta P_{\mathrm{load}}(t) \Delta t, P_{\mathrm{int\_load\_max}}\right). \end{aligned} \tag{30}$$

The upward adjustment flexibility index is defined as follows:

$$f_{\text{up}}(t) = \frac{P_{\text{demand\_up}}(t)}{P_{\text{supply\_up}}(t)}. \tag{31}$$

When $f_{\text{up}}(t) < 1$, it indicates that $P_{\text{supply\_up}}(t) > P_{\text{demand\_up}}(t)$ and a certain margin of flexible resources exists.

The downward flexibility index is defined as follows:

$$f_{\text{down}}(t) = \frac{P_{\text{demand\_down}}(t)}{P_{\text{supply\_down}}(t)}. \tag{32}$$

When $f_{\text{down}}(t) > 1$, the flexible resources do not meet the grid demand and wind and PV curtailment is needed to ensure the balance of supply and demand of flexible resources.

To facilitate the calculation, the upward and downward flexibility indices are combined into a system flexibility index.

$$\begin{aligned} f_{\text{flex}} &= \xi \sum_{t=1}^{T} f_{\text{up},t} + (1-\xi) \sum_{t=1}^{T} f_{\text{down},t}, \\ \xi &= \frac{\sum_{t=1}^{T} P_{\text{demand\_}up}(t)}{\sum_{t=1}^{T} \left(P_{\text{demand\_up}}(t) + P_{\text{supply\_up}}(t) \right)}. \end{aligned} \tag{33}$$

This index and the daily operating cost and flexibility compensation cost are passed to the upper level for iterative calculations.

3.5. Solution Method. Taking into consideration that the control variables of the upper-level model are discrete and the variables of the lower-level model are continuous, the upper-level planning sub-problem is solved by the NSGA-II [22]. It is a non-dominated ranking genetic algorithm using an elite strategy that can find a set of Pareto-optimal solutions within a limited number of iterations. The lower-level planning uses a linear programming algorithm for the day-ahead scheduling to obtain the optimal operational solution for a typical day.

In this study, the population size of the algorithm is set as 10 and the number of generations is set as 100. The crossover rate and the mutation rate is 0.9 and 0.1, respectively. The steps of the solving algorithm of the model are shown in Figure 2.

In the upper-level model, there are mutually constraining relationships between economics and flexibility. On one hand, the operational flexibility is essential for the system to effectively handle the unpredictable fluctuations in the net load curve. If only considers the economic cost, there may be a potential for underestimating the capacity of the flexibility resource. On the other hand, the allocation of resources aimed at meeting the flexibility of the system may result in high investment costs. It is necessary to calculate weight coefficients for the traditional method of combining multiple objectives into a single objective function. The NSGA-II adopted in this paper has three major advantages, including nondominated sorting, crowding distance, and elite preserving strategy, which can effectively solve the problem without setting the weight coefficients of economics and flexibility.

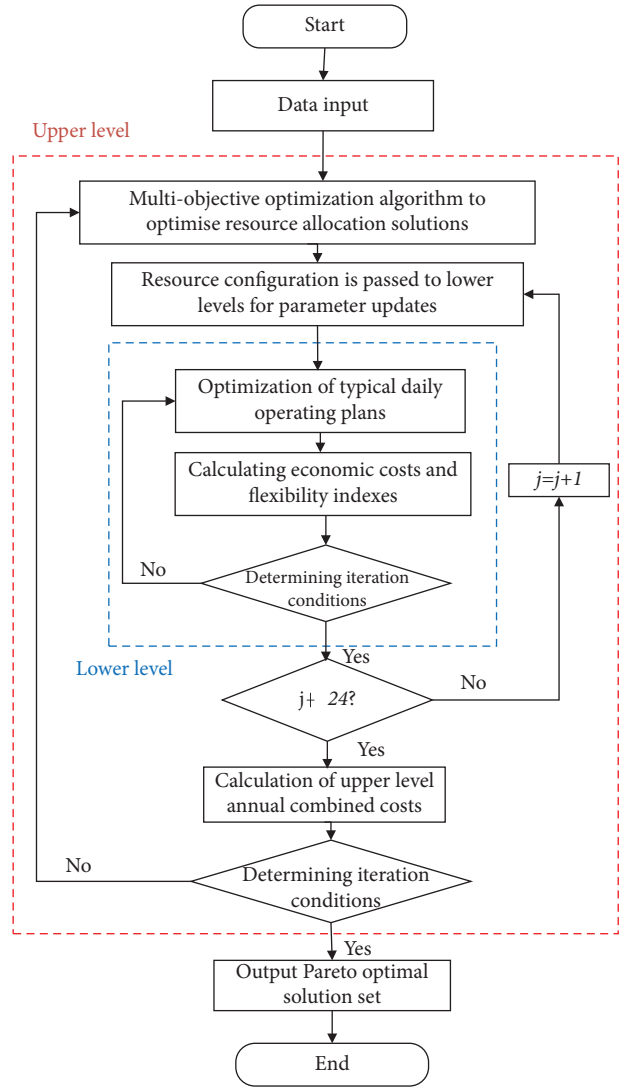

Figure 2: Algorithm-solving process.

4. Case Study

4.1. Input Data. The effectiveness of the proposed method is verified by applying a practical power system in the southern province of China. In this section, based on the bilevel operation-planning joint optimization model proposed above, the case study is on a planning horizon of 15 years and is to optimize the flexible capacity allocation in a province. Combining the actual resource situation, investment cost, and demand of various flexible resources, the unit investment and operation cost of flexible resources are shown in Table 1, and the planning upper and lower limits of each resource in the planning years are shown in Table 2. Also, the weights of gas-fired and coal-fired units, thermal units' flexibility transformation, hydropower, energy storage, pumped storage, and interruptable load are set as 0.1, 0.15, 0.25, 0.15, 0.1, 0.2, and 0.05, respectively.

Table 1: Unit costs for various types of flexible resources.

Flexible resources	Unit investment cost ($\times 10^4$yuan/MW)	Unit operating cost ($\times 10^4$yuan/MWh)
Gas units	40	0.66
Coal-fired units	500	0.32
Thermal power unit flexibility retrofit	120	0
Hydro	1000	0
Pumped hydro storage	800	0.06
ESS	150	0.045
Interruptable load	100	0.66

Table 2: Capacity for each type of flexibility resource.

Flexible resources	Minimum capacity ($\times 10^4$ kw)	Maximum capacity ($\times 10^4$ kw)
Gas units	350	386
Coal-fired units	3000	3500
Thermal power unit flexibility retrofit	0	1100
Hydro	1220	1236
Pumped hydro storage	240	500
ESS	120	400
Interruptable load	1348	2800

4.2. Typical Day Selection. Since the renewable energy output fluctuates greatly and has a greater impact on the differential distance clustering, the curve smoothing process is first performed on the output data of wind and PV using the polynomial difference method to attenuate large fluctuations and further reflect the overall trend of the curve. Taking the output of wind power, PV, and load data of a practical town area for net load calculation, sampling the data at the same time interval for each day, the final data can be obtained.

Since there is an order of magnitude difference between the measurements of different scales, thus leading to an inaccurate description of the overall morphological features, so the entropy weight method is introduced to determine the objective weights resulting in $\alpha = 0.0179$, $\beta = 0.0009$, $\gamma = 0.9339$, and $\rho = 0.0473$, and the final clustering results are shown in Figure 3. The red line in the figure is the typical day, and the black is the curve of net load with similar morphological characteristics. The number of the first sample is 214, the second is 24, the third is 51, and the fourth is 76.

The number of clusters is set as 4, and the net load curves of 365 days in a year are divided into 4 categories by clustering. The four selected typical days are shown in Figure 4, which is a typical day selected as day 107, day 116, day 230, and day 349 in the original data.

4.3. Analysis of Optimized Flexible Capacity Allocation Results. The set of Pareto-optimal solutions obtained by the proposed algorithm is shown in Figure 5. Each point represents an allocation case of the flexible resources. According to the nondominated nature of the Pareto principle, there is no superiority or inferiority among each flexible capacity allocation solution.

The distribution of Pareto solutions shows the correlation between the economic and flexibility metrics and provides various cases. The capacity of the flexibility resource corresponding to each capacity allocation case is shown in Table 3.

Among the cases considered, case 1 focuses more on flexibility, while case 4 is less flexible due to an excessive focus on low cost. Case 2 and case 3 have similar flexibility, but case 3 is more economical. Therefore, case 3 is the best option. Comparison of the results shows very little change in the capacity of gas units and ESS, mainly due to the limited planning of gas units and the higher investment costs of ESS.

Flexibility rises as the investment in renewable energy high penetration power systems increase. Case 1 and case 2 benefit from the investment in more flexible resources to improve flexibility of the system. It is obvious that the annual operating cost causes the difference between the annual combined costs of the four cases as shown in Figure 6. Compared to case 1, which displays lower flexibility and higher operating costs, case 3 and case 4 demonstrate a higher level of flexibility and a reduction in operating costs.

4.4. Power Balance Analysis. The power balance of the lower-level model is analyzed. Case 3 is selected as the flexible capacity allocation option. The results are shown in Figure 7, where the output of each flexibility resource in the system meets the objective of optimal economics and flexibility. Considering that the hydropower output is affected by the water quantity, simulations are conducted for two typical days in dry and wet seasons. It can be found that the hydropower output increases significantly in the wet season.

From Figure 8, it can be seen that with the known resource allocation scheme, both the upward flexibility index and the downward flexibility index satisfy the conditions,

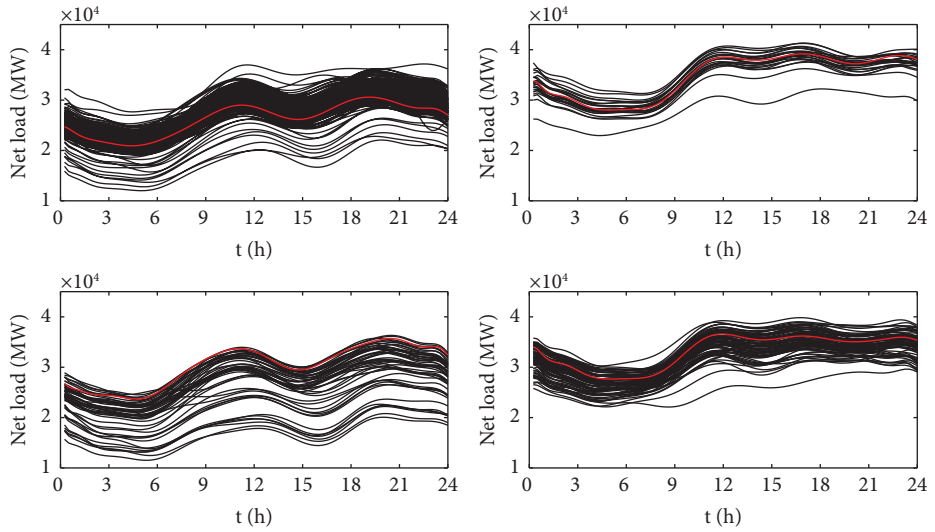

Figure 3: Typical day selection of the net load based on curve shape clustering.

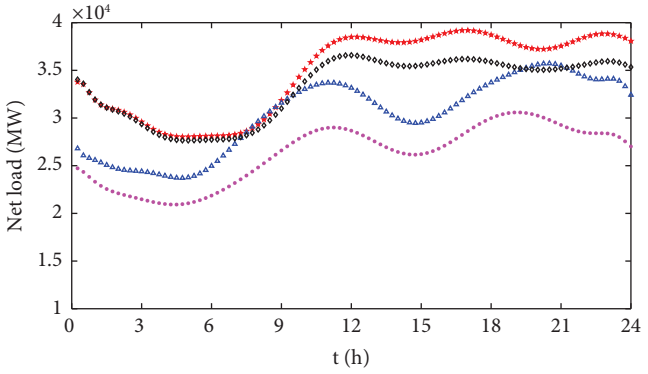

Figure 4: Net load clustering centrality curve.

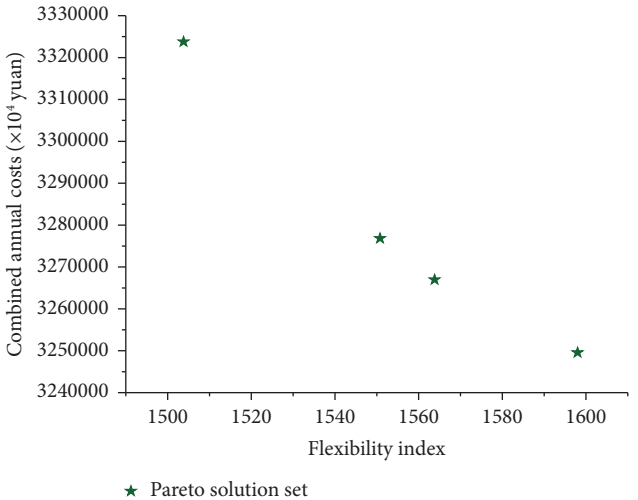

Figure 5: Pareto frontier diagram for flexible capacity allocation.

Table 3: The result of flexible capacity allocation.

Flexible resources	Case 1 (MW)	Case 2 (MW)	Case 3 (MW)	Case 4 (MW)
Gas units	3632	3629	3616	3618
Coal-fired units	32233	31540	31006	30967
Thermal power unit flexibility retrofit	12211	12211	12235	12263
Hydro	3908	4570	4674	4980
Pumped hydro storage	1380	1602	3023	3678
ESS	2124	2126	2156	2175
Interruptable load	339	200	90	83

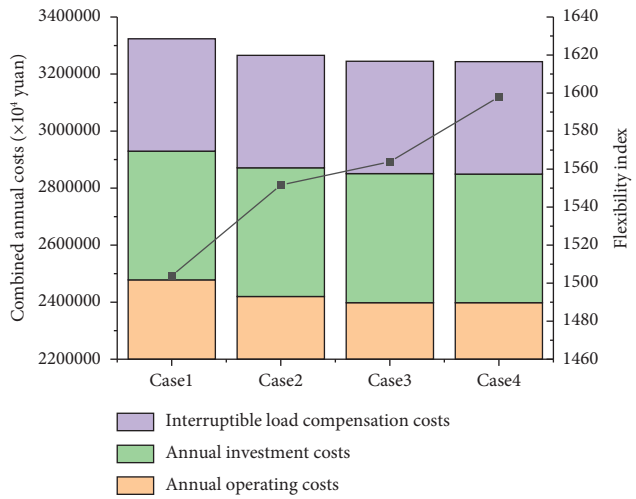

Figure 6: Comparison of the combined annual cost and flexibility index.

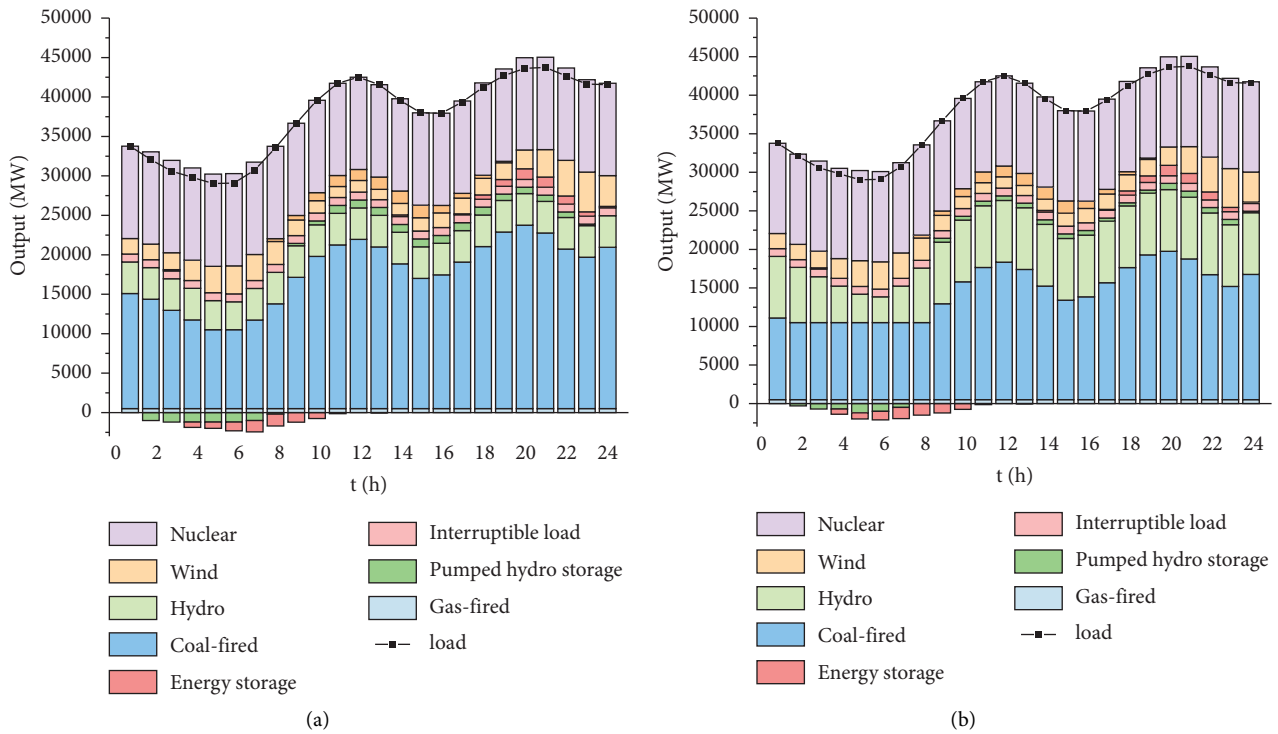

Figure 7: Output of flexible resources in case 3. (a) Typical day 2 (dry season). (b) Typical day 3 (wet season).

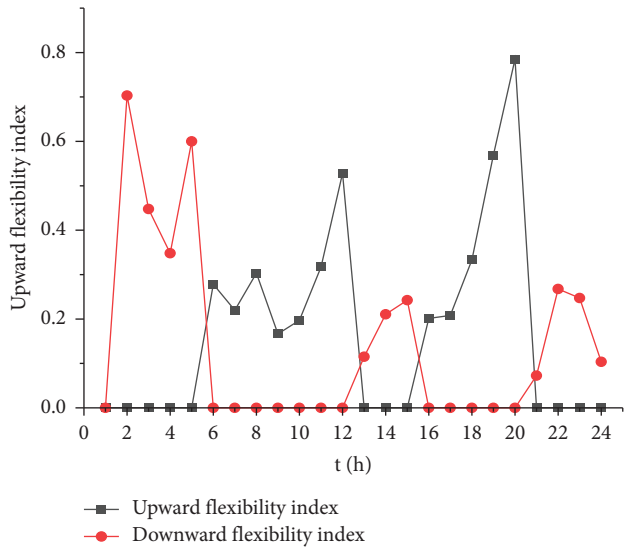

Figure 8: Flexibility index for typical day 2 in case 3.

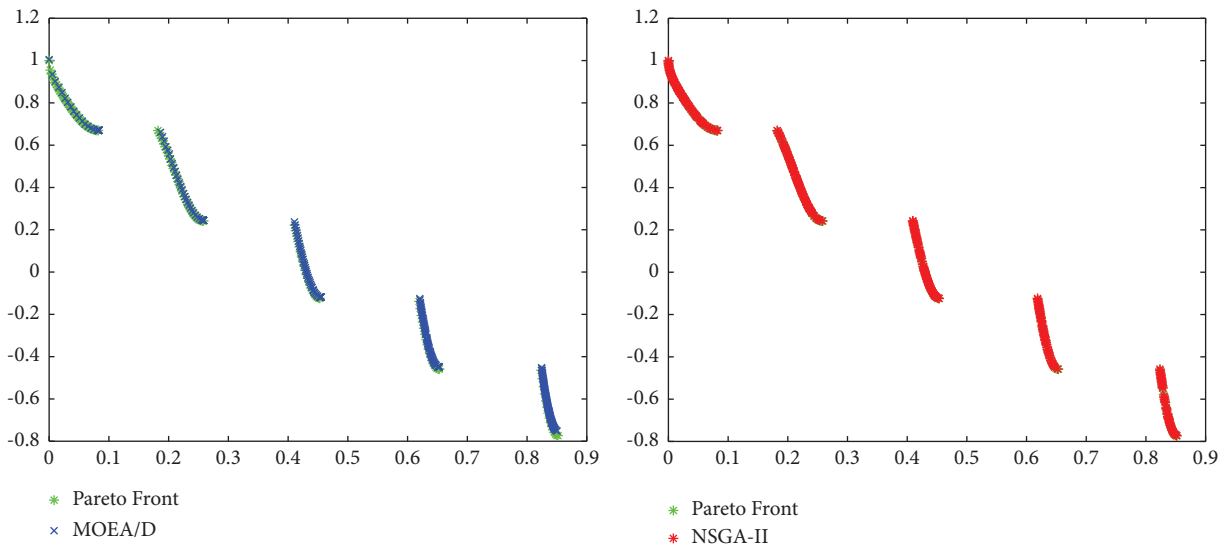

Figure 9: Comparison of MOEA/D and NSGA-II algorithms for Pareto optimal solution with ZDT3 function. (a) Solution of MOEA/D compared with the Pareto front. (b) Solution of NSGA-II compared with the Pareto front.

indicating that the configuration meets the grid demand and there is a certain margin of flexible resources.

Through recursive iteration between the upper and lower layer, the collaboration between multi-objective planning and optimization operations can be achieved so that the planning scheme solved by the model in this paper becomes more realistic.

4.5. Algorithm Performance Results. Considering that the decision variable in the upper level is the capacity of the flexibility resource, the comparison between the algorithms MOEA/D and NSGA-II is conducted using the ZDT3 function, which has a discrete Pareto front. The objective function of ZDT3 is as follows:

$$f_1(x) = x_1,$$

$$f_2(x) = g(x)\left[1 - \left(\frac{f_1(x)}{g(x)}\right)^2\right],$$

$$g(x) = 1 + \frac{9}{n-1}\sum_{i=2}^{n} x_i, \quad x_i \in [0,1], i = 1,2,\ldots,n, n = 30. \tag{34}$$

Table 4: The algorithm performance comparison between MOEA/D and NSGA-II.

Algorithms	Solution time (s)	**D**-matrix
NSGA-II	105.52328	0.00189
MOEA/D	14.82179	0.00541

The population size of algorithms is set as 100, and the number of generations is set as 250. The crossover rate and the mutation rate of the NSGA-II is 0.9 and 0.1, respectively. Each comparison experiment runs 5 times, and the results of the experiment with the smallest selected D matrix are shown in Figure 9. The D matrix evaluates the overall performance of a population by calculating the distance between the population and the optimal Pareto front [23].

Figure 9 compares the distribution of Pareto optimal solutions for the NSGA-II and MOEA/D algorithms. The solution of NSGA-II is almost completely consistent with the Pareto front. It is obvious that in the ZDT3 problem, a larger set of solutions generated by NSGA-II outperforms that obtained by MOEA/D.

Comparing the solution time of the algorithm to solve the same ZDT3 as shown in Table 4, the solution time of MOEA/D is shorter than NSGA-II. While from the **D**-matrix, it can be seen that the distances obtained by MOEA/D are relatively larger than those by NSGA-II. It means that the uniformity of solution distribution of NSGA-II is better than that of MOEA/D. Consequently, better results of the ZDT3 can be obtained by NSGA-II than MOEA/D.

5. Conclusions

A bi-level operation-planning joint optimization model based on morphological clustering for the selection of typical options is proposed in this paper. The aim is to improve the ability of power system to maintain the economics and flexibility of the system.

The multitimescale fluctuation of high renewable penetration power systems poses challenges on the flexible operation of the system. To tackle the challenge and improve the efficiency of capacity allocation, a morphological clustering algorithm based on the multiscale and entropy weight method is proposed. The traditional Euclidean distance is replaced by the curvilinear morphological distance for the selection of typical scenarios of flexibility demand.

The test results of the case study verify the validity and rationality of the bilevel operation-planning joint optimization model for flexible capacity allocation. The model is able to achieve the collaborative optimization and the overall economics and flexibility through a finite number of recursive iterations. The obtained flexible capacity allocation scheme can meet the flexibility needs and keep the supply-demand balance of the power system.

This paper only takes into account the flexible resources of the source-load storage. In order to further improve the flexibility of high renewable penetration power system, the complex model in this paper can be extended to include other flexibility sources such as the transmission network.

Data Availability

The data used to support the findings of this study have not been made available because of privacy.

Conflicts of Interest

The authors declare that they have no conflicts of interest.

Acknowledgments

This work was funded by the Shanghai Sailing Program (no. 21YF1414700).

References

[1] H. Chen, K. Gao, S. Tian, R. Sun, K. Cui, and Y. Zhang, "Nexus between energy poverty and sustainable energy technologies: a roadmap towards environmental sustainability," *Sustainable Energy Technologies and Assessments*, vol. 56, 2023.

[2] Iea, "Status of Power System Transformation 2019: Power System Flexibility," Reports, International Energy Agency, Paris, France, 2019.

[3] W. Pan, C. Zhao, L. Fan, and S. Huang, "Efficient optimal power flow flexibility assessment: a machine learning approach," in *Proceedings of the 2023 IEEE Power and Energy Society Innovative Smart Grid Technologies Conference (ISGT)*, pp. 1–5, Washington, DC, USA, March 2023.

[4] Z. Lu, H. Li, and Y. Qiao, "Probabilistic flexibility evaluation for power system planning considering its association with renewable power curtailment," *IEEE Transactions on Power Systems*, vol. 33, no. 3, pp. 3285–3295, 2018.

[5] M. Saffari, M. McPherson, and A. Rowe, "Evaluation of flexibility provided by cascading hydroelectric assets for variable renewable energy integration," *Renewable Energy*, vol. 211, pp. 55–63, 2023.

[6] Y. Zhao, M. Liu, C. Wang, X. Li, D. Chong, and J. Yan, "Increasing operational flexibility of supercritical coal-fired power plants by regulating thermal system configuration during transient processes," *Applied Energy*, vol. 228, pp. 2375–2386, 2018.

[7] S. O. Gardarsdòttir, L. Göransson, F. Normann, and F. Johnsson, "Improving the flexibility of coal-fired power generators: impact on the composition of a cost-optimal electricity system," *Applied Energy*, vol. 209, pp. 227–289, 2018.

[8] L. Baringo and A. Baringo, "A stochastic adaptive robust optimization approach for the generation and transmission expansion planning," *IEEE Transactions on Power Systems*, vol. 33, no. 1, pp. 792–802, 2018.

[9] X. Wang, R. Yu, L. Zhang, and N. Chen, "A method for optimal allocation of source-load-side flexible resources considering the demand of peaking scenarios," in *Proceedings of the 2022 7th International Conference on Power and Renewable Energy (ICPRE)*, pp. 572–576, Shanghai, China, September 2022.

[10] P. Li, Z. Wang, H. Liu, J. Wang, T. Guo, and Y. Yin, "Bi-level optimal configuration strategy of community integrated energy system with coordinated planning and operation," *Energy*, vol. 236, 2021.

[11] J. Li, B. Lu, Z. Wang, and M. Zhu, "Bi-level optimal planning model for energy storage systems in a virtual power plant," *Renewable Energy*, vol. 165, pp. 77–95, 2021.

[12] H. Wang, J. Hu, D. Dong et al., "Research on evaluation of multi-timescale flexibility and energy storage deployment for the high-penetration renewable energy of power systems," *Computer Modeling in Engineering and Sciences*, vol. 134, no. 2, pp. 1137–1158, 2023.

[13] Z. Huang, Z. Xie, C. Zhang et al., "Modeling and multi-objective optimization of a stand-alone PV-hydrogen-retired EV battery hybrid energy system," *Energy Conversion and Management*, vol. 181, pp. 80–92, 2019.

[14] S. Verma, M. Pant, and V. Snasel, "A comprehensive review on NSGA-II for multi-objective combinatorial optimization problems," *IEEE Access*, vol. 9, pp. 57757–57791, 2021.

[15] F. Nie, Z. Li, R. Wang, and X. Li, "An effective and efficient algorithm for K-means clustering with new formulation," *IEEE Transactions on Knowledge and Data Engineering*, vol. 35, no. 4, pp. 3433–3443, 2023.

[16] A. M. Ikotun, A. E. Ezugwu, L. Abualigah, B. Abuhaija, and J. Heming, "K-means clustering algorithms: a comprehensive review, variants analysis, and advances in the era of big data," *Information Sciences*, vol. 622, pp. 178–210, 2023.

[17] Q. Zhu, X. Bian, P. Lou, and Z. Tang, "Morphological clustering algorithm of daily output curve of wind farm based on multi-scale and entropy weight method," in *Proceedings of the 2021 Int. Top-Level Forum on Engineering Science and Technology Development Strategy*, pp. 549–564, Springer, Singapore, March 2022.

[18] S. Liu, Y. Liu, C. Yang, and L. Deng, "Relative entropy of distance distribution based similarity measure of nodes in weighted graph data," *Entropy*, vol. 24, no. 8, p. 1154, 2022.

[19] C. Zhu, "The local variational principle of weighted entropy and its applications," *Journal of Dynamics and Differential Equations*, vol. 34, 2022.

[20] C. Qiao and W. Zhang, "Research on classification method of CRH maintenance parts based on entropy weight-clustering analysis," in *Proceedings of the 2019 IEEE 8th Joint International Information Technology and Artificial Intelligence Conference (ITAIC)*, pp. 517–521, Chongqing, China, May 2019.

[21] R. B. H. Ahmed, A. Bouzir, and S. Benammou, "Measuring the competitiveness of mediterranean ports via the principal component analysis and hierarchical clustering analysis methods," in *Proceedings of the 2020 IEEE 13th International Colloquium of Logistics and Supply Chain Management (LOGISTIQUA)*, pp. 1–6, Fez, Morocco, February 2021.

[22] N. Huanna, Y. Lu, Z. Jingxiang, W. Yuzhu, W. Weizhou, and L. Fuchao, "Flexible-regulation resources planning for distribution networks with a high penetration of renewable energy," *IET Generation, Transmission and Distribution*, vol. 12, no. 18, pp. 4099–4107, 2018.

[23] X. Zhang, "A new decomposition-based many-objective algorithm based on adaptive reference vectors and fractional dominance relation," *IEEE Access*, vol. 9, pp. 152169–152181, 2021.